A Mobile Security Robot equipped with UWB-Radar for Super-Resolution Indoor Positioning and Localisation Applications

Rahmi Salman
Fachgebiet Nachrichtentechnische Systeme
Universität Duisburg-Essen
47057 Duisburg, Germany
salman@nts.uni-due.de

Ingolf Willms
Fachgebiet Nachrichtentechnische Systeme
Universität Duisburg-Essen
47057 Duisburg, Germany

***Abstract*—In this paper an autonomous mobile security robot named CoLORbot is introduced which operates with UWB-Radar technology. The objective is the 2D inspection of an unknown indoor area with randomly distributed unknown solitary objects. Environmental imaging by means of electro-magnetic wave propagation in the mm range is performed. Different sensor configurations (mono-static vs. bi-static) and different antenna designs (omni-directional pattern vs. narrow beam directive pattern) are evaluated and analysed. The CoLORbot which is fully equipped with professional motion units, UWB-Radar devices, antennas and a laptop for data processing is introduced and evaluated. Strategies to perform this kind of multi disciplinary purpose containing challenges in robotics, UWB-Radar sensing, imaging algorithms and antenna handling are revised and in every case experimentally validated.**

Keywords- Environmental Imaging; Super-resolution; UWB-Radar; UWB imaging; UWB based position determination.

I. INTRODUCTION

On March 11, 2011 a 9.0 earthquake and subsequent tsunami hit the Fukushima Daiichi nuclear power plant and led to the world's most fatal nuclear disaster since Chernobyl. 150.000 people had to flee their homes because of radiation contamination. It took 5 weeks before the first remote controlled security robot could enter the reactor building to provide interior images of the scenario which was too dangerous for the security forces to enter. Neither Japan, which was known until then to be a leading nation in robotics, nor any other country was able to provide security robots to operate in hazardous scenarios full of dark dense smoke, dust and other particles. Throughout the inspections all robots were equipped with spotlights to enable optical sensors.

This tragic example shows more than ever the need of pioneering sensing technologies which overtop or at least complement the classical sensors like optics, infrared, ultrasound and narrowband Radars. UWB technology has superior potential compared to these technologies. Henceforth, it is possible not only to sense in dense smoke and dust filled scenarios but even to deeply penetrate dielectric material due to the presence of low frequencies. Combined with high temporal and spatial resolution due to the huge bandwidth UWB-Radar provides a certain degree of multipath immunity. Because of these hard facts and many more (low power emission, co-existence with narrow band radio systems, small and cost effective devices etc.) UWB-Radar revolutionised the understanding of Radar. Radar applications not only increase the quantity of information for the end-user but rather the quality of information which enables new dimensions in the field of short-range indoor sensing [1][2].

II. HARDWARE SETUP

The main focus of this paper is placed on a robust transfer of the algorithms [2] from laboratory conditions to a more realistic indoor propagation scenario using the robot. With regard to final experimental validations immense hardware effort concerning a mobile robot was performed in a realistic complex indoor scenario and several solitary objects were designed and set up.

A. *Indoor Measurement scenario*

The ground plane of the investigated indoor scenario is depicted in the top Fig. 1.

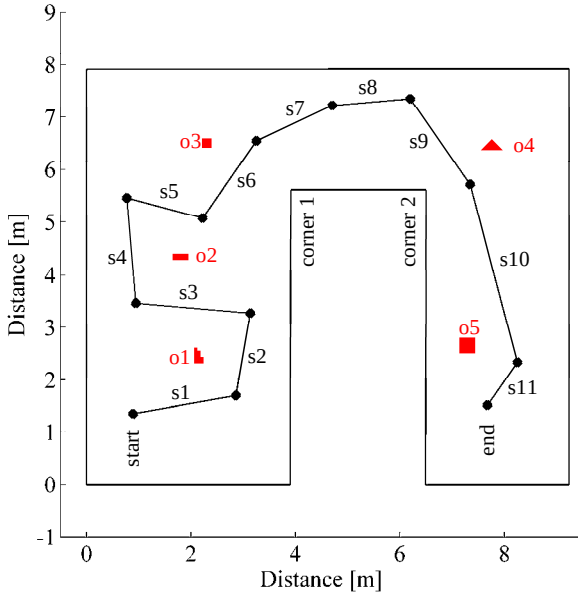

978-1-4673-1954-6/12/$31.00 ©2012 IEEE

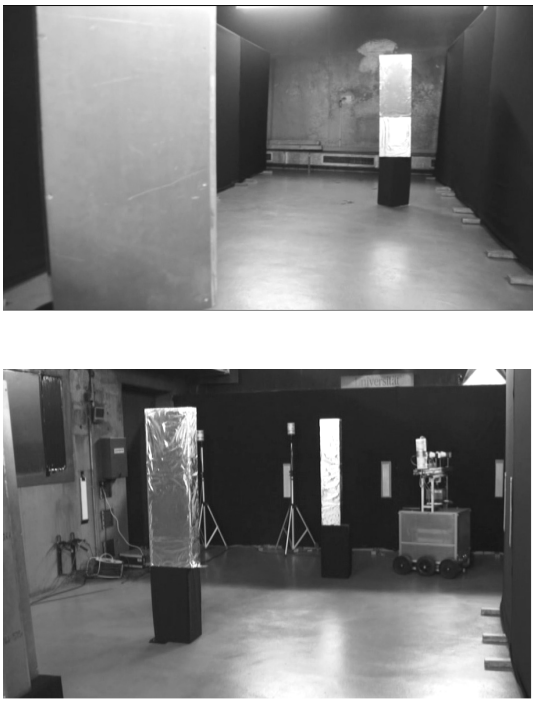

Figure 1. Schematic drawing and photographs of the measurement location

To provide a realistic and not too simple indoor scenario with corners as well as edges and dimensions (56m^2) like that of a larger office room, the fire detection laboratory of the University Duisburg-Essen was modified and used as the location for the measurement campaign. The modification consists of partly installed portable metallic walls to give the room a more complicated shape and to hide several lab devices from the influences to the UWB-Radar measurements. To compare the performance of different antennas with different configurations the robot's track which consists of 11 straight segments was not changed throughout the investigations. The length of each segment is s1 = 2m, s2 = 1.6m, s3 = 2.2m, s4 = 2m, s5 = 1.5m, s6 = 1.8m, s7 = 1.6m, s8 = 1.5m, s9 = 2m, s10 = 3.5m and s11 = 1m. Further, to analyse the influence of the track, which finally generates the synthetic aperture, the first 6 segments exhibited different orientations making the track more chaotic by then. Whereas the rest of the segments (s7-s11) are more or less quite linear in their orientation. 5 objects with cross sections up to 0.3m were distributed in the scenario, which are depicted in red in Fig. 1 with original dimension. However, in environmental imaging applications with non-ideal sensor tracks these objects can hardly be classified in detail. This would require a full or at least a restricted circular track in short range with aligned sensors to gather high-resolution contour information. In that sense, a detailed figure of the used objects would not provide any further information and is skipped here.

B. The Mobile Security Robot CoLORbot

An autonomous mobile security robot with professional motion units was fully equipped with UWB-devices, RF components, a power supply unit and a laptop for data acquisition and communication with the data fusion computer. Schematic drawings of the robot as well as photographs are provided in Fig. 2.

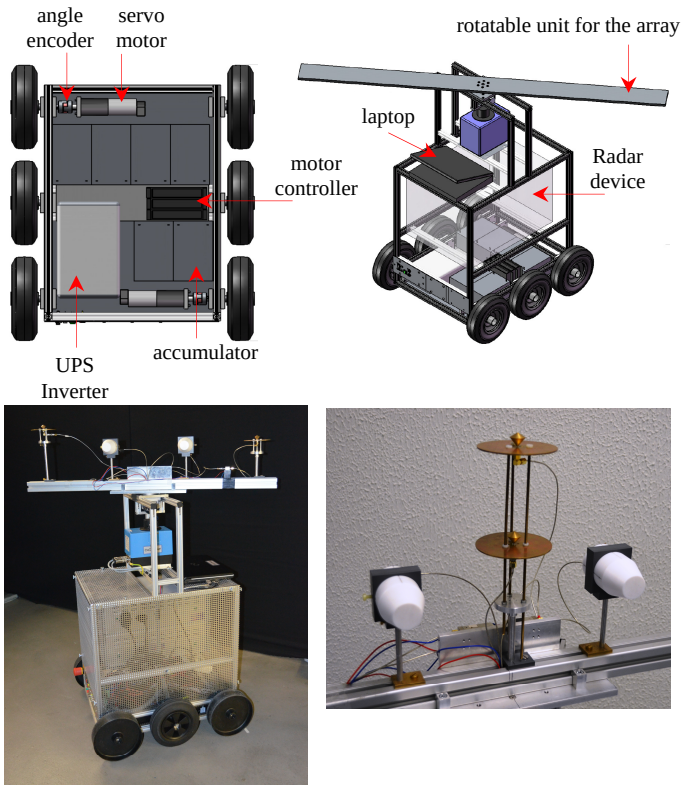

Figure 2. The mobile security robot CoLORbot and the used antenna array in bi-static (bottom left) and quasi mono-static configuration (bottom right)

Localisation and positioning accuracy by means of UWB-Radar is predominantly achieved by advanced algorithms [3]. If a mobile security robot is intended to assist this operations the design and equipment of the robot has to fulfil certain demands concerning motion accuracy. Therefore, some specifications have also been taken into account. There are totally three actuators in the robot, two in the motion unit at the bottom and one at the top which rotates the actual antenna array. The actuators are all hollow-shaft servo motors, which offer unique features unsurpassed by conventionally geared drives. Used in highly demanding industrial and medical servo systems they provide outstanding precision motion control and high torque capacity in a very compact package. Additionally, the gear ratio is set to 1:150 and is combined with a supplementary angle encoder with 500 Ticks per turn. This results in a sampling rate of 75000 samples per rotation for each actuator. The robot has 3 solid rubber tires at both sides which are connected by a chain-drive. To maintain a more gliding rotation of the robot with reduced errors the circumference of the middle tire is minimally higher than those of the other ones. The dimensions of the robot as well as the tire position maintain a rotation centre in the middle of the robot which also equals the middle of the antenna array at the top. Hence, the movement of the robot was entirely restricted to translations and rotations, strictly avoiding curvature paths. As mentioned previously, to further minimize erroneous robot

motions the antenna array is equipped with its own rotational unit. The antenna alignment can be performed by just rotating the array, which is preferred compared to rotating the whole robot in case of an uneven floor.

C. Radar Device and Antennas

The used Radar system consists of a UWB Maximum Length Binary Sequence (M-Sequence) Radar system [4] with an operating band of DC–4.5 GHz. For higher time resolution an additional quadrature modulator was used which operates with a carrier frequency of 9 GHz and doubles the bandwidth. Thus, the operating frequencies occupy the band of 4.5 GHz up to 13.5 GHz with an absolute bandwidth of 9 GHz and a fractional bandwidth of 100%.

Two types of UWB antennas were used within these paper, i.e. an omni-directional mono-cone antenna and a directive Teflon embedded two tapered slot line Vivaldi antennas on a single substrate. The mono-cone antenna has an omni-directional radiation pattern in azimuth range which performs in the range of 3 GHz up to 14 GHz with an antenna gain of 2 dBi. The Vivaldi antenna performs in the same band with an antenna gain of up to 15 dBi and a narrow 3dB beam width of 25°. Both antennas have a satisfying matching with an s-parameter s11 less than 10dB in the whole range. The directive Vivaldi antennas were used throughout in bi-static configuration with 30 cm distance between each other and symmetrically placed around the rotation centre of the robot. The omni-directional antennas were either used in bi-static configuration (80 cm distance and symmetrically placed around the rotation centre) or in a quasi mono-static configuration placed one upon each other aligned in the rotation centre. Both setups can be seen in Fig. 2.

III. Environmental UWB-Radar Imaging

Environmental inspection by means of electromagnetic waves which are transmitted and received by a mobile security robot is based on synthetic aperture Radar (SAR) principles. Instead of using one sensor with a large real aperture, the motion of the sensors generates a synthetic aperture. Here, the CoLORbot was used with a speed of approximately 1 m/minute with a pulse repetition rate of 15 pulses/second. Within this inspection tour the environment interacts with the transmitted UWB pulses and is characterised by diffraction, reflection, and scattering. These effects are determined by the geometry of the objects, the operating frequency, the material composition and the polarisation of the incident wave. Within this paper the geometry of the environment shall be analysed and the remaining parameters are assumed to be constant or negligible. Thus, all received pulses have to be processed concerning their spatial and temporal signature subject to the local coordinate of the point of acquisition.

The imaging algorithm used in this work is Kirchhoff migration (KM). KM is a basic imaging algorithm which is extensively analysed in the literature. The application of KM assumes Rayleigh scattering radiation which is fulfilled only if the size of the objects is much smaller than the used wavelength. Otherwise artefacts occur which distort the resulting image to some extent. However, due to its low complexity and therewith simple adaption to given scenarios KM is widely used in the UWB-Radar community. The main idea is a back projection of the radiation characteristic and relies on some form of coherent summation. This means that a pixel of the Radar image is produced by integrating the phase-shifted Radar data of each antenna position. N measurements contribute to the value of a pixel with (x,y)-coordinate which can be mathematically formulated as

$$p(x,y) = \frac{1}{N}\sum_{n=1}^{N} h_n\left(\frac{d_{TXn} + d_{RXn}}{c_0}\right). \tag{1}$$

Here, h_n is the n-th measured impulse response in time domain, d_{TXn} and d_{RXn} are the distances between the (x,y)-coordinate and the transmit and receive antenna, respectively. The speed of light is c_0. In case of a bi-static configuration this algorithm summarises the impulse response values along ellipses (circles in mono-static configuration). At positions where objects cause a reflection and therewith increase the values in the impulse response the ellipses superpose to image spots of high intensity. The image contrast is higher with increasing number of recorded impulse responses at different positions.

However, the superposition also leads to image artefacts because the ellipses do not only intersect at object locations. Hence, this ambiguity of intersection of ellipses decreases the spatial resolution and causes erroneous hot spots. Moreover, even in image area where the ellipses do not intersect the noise floor is increased by the ellipses themselves which reduces the signal to noise and signal to clutter ratio. These artefacts occur more strongly with omni-directional antennas because of their isotropic radiation pattern and the lower antenna gain. To some extent and under special circumstances (dense clutter with positions near to objects of interest) theses artefacts can make the interpretation of the resulting image difficult or even impossible.

To overcome these artefacts a modification of the KM called cross-correlation back projection was proposed in [5]. The principle of this algorithm is that the intensity of an image pixel does not consist of Radar data any more but rather of correlation coefficients of a correlation operation with a reference measure. This can be expressed by

$$p(x,y) = \frac{1}{N}\sum_{n=1}^{N}\int_{-\frac{T}{2}}^{\frac{T}{2}} h_n\left(\frac{d_{TXn} + d_{RXn}}{c_0} + \psi\right) h_{\mathrm{ref}}\left(\frac{d_{TX\mathrm{ref}} + d_{RX\mathrm{ref}}}{c_0} + \psi\right)\mathrm{d}\psi. \tag{2}$$

Here, the argument of h_{ref} is aligned with the area of interest, i.e. the coordinates of the pixel $p(x,y)$.The correlation operation is finally carried out by averaging over the pulse duration T. The correlation coefficients result in nonzero samples only when the ellipse of the reference pulse crosses with the ellipse of the sensor position under test. This drastically reduces the risk of superimposing pixels to phantom hot spots. However, the performance of the cross-correlation

back projection extremely depends on the local selection of the reference node. The more orthogonal the impulse responses of the measurement under test and the reference measurement are the more enhanced is the resulting image with higher dynamic range and less phantom pixels. Or in other words, if the reference track and the track under test have similar orientations the resulting image converges to the image obtained by classical migration. This makes the application of cross-correlation back projection difficult in real emergency scenarios. A reference node can simply be chosen of one of the previous measurements but for satisfying results this assumes a more chaotic track which may not be possible in every time due to the infrastructure of hazardous scenarios.

IV. IMAGE PROCESSING RESULTS

In this chapter results are shown of the evaluation of previously mentioned imaging algorithms with given hardware equipment mentioned in the second chapter. But before, to focus on the purpose of this paper the challenges and main idea shall be briefly recaptured.

Environmental imaging in unknown indoor scenarios with randomly distributed solitary objects addresses following challenges:

- Due to the stationarity there is no speed difference between targets and the background.
- Unknown scenarios provide no background information which complicates the distinction of targets of interest and clutter.
- Indoor scenarios may result in dense clutter distribution. In worst case clutter occurs spatially close to targets of interest.

Once a rough map or partial map is built valuable information can be gathered for the autonomous orientation, positioning and navigation of the robot for further (detailed) inspections.

A. Performance Analysis of the Omni-Directional Antennas

During the investigations in this chapter both omni-directional antennas are analysed regarding their configuration. In both cases the array itself keeps static. The CoLORbot moves straight forward along the 11 segments and changes its orientation between each segment. Throughout the movement the Radar device sequentially records pulses which are processed by the previously mentioned classical KM algorithm.

a) Quasi Mono-Static Configuration

For the quasi mono-static configuration the antenna array is equipped with both omni-directional antennas mounted one above each other (see Fig. 2, bottom right) and aligned with the rotation centre. The result can be seen in Fig. 3. Here, a fixed meshgrid of 11m x 11m is processed for each sensor position and superimposed gradually. As mentioned previously, both main drawbacks of KM heavily occur - there are a lot of phantom artefacts and the dynamic range is drastically low. The image is by far hard to interpret.

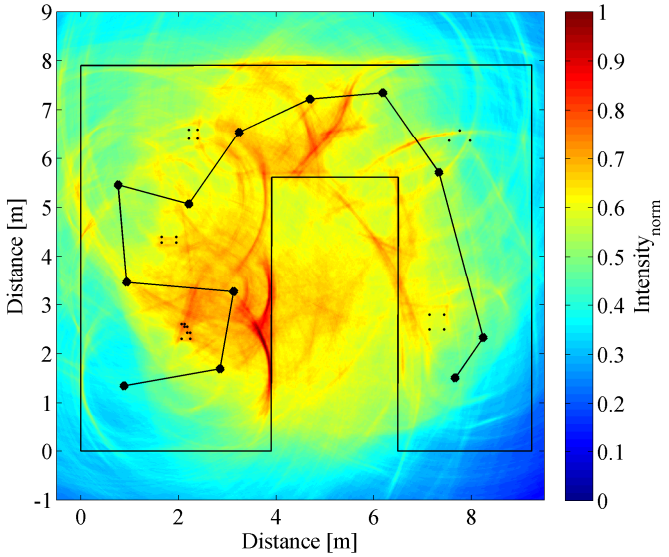

Figure 3. Full image with the omni-directional antennas in quasi mono-static configuration

b) Bi-Static Configuration

For the bi-static configuration the antenna array is equipped with both omni-directional antennas each separated by a distance of 0.4m to the rotation centre (see Fig. 2, bottom left). The measurement setup as well as the processing remain unaffected to provide a meaningful comparison. The result is depicted in Fig. 4.

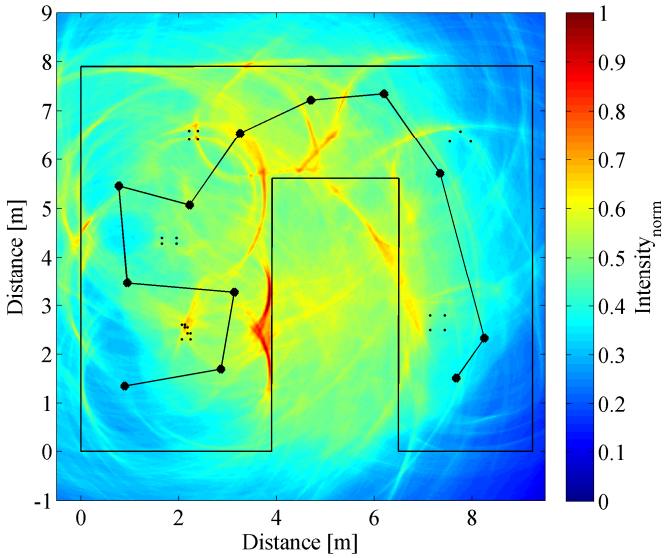

Figure 4. Full image with the omni-directional antennas in bi-static configuration

The bi-static configuration provides increased dynamic range. The signal to noise and signal to clutter ratio is visibly enhanced by just separating the antennas by a distance of 0.8m from each other. However, phantom hot spots still remain, e.g. around corner 1, s6 and s7. This enhancement is not explained by different antenna crosstalk patterns, because the crosstalk is every time removed by a window-function within the

framework of pre-processing. To some extend the enhancement can be explained because in case of the quasi mono-static configuration the lower antenna is shadowed partially by the arrangement of rods to fix the construction. In larger part the reason is the exploitation of more viewing and illumination angles which are available in the bi-static configuration provided by the spatial diversity.

c) Clustered Image Processing

However, in order to exploit further improvement it does not make any sense to perform the KM for such a large-scale dimension (although it is widely seen in the literature). It is more appropriate, to image the adjacent area around the robot and not for several metres. This leads to higher dynamic range because the noise floor is not increased by distant and irrelevant positions. Moreover, phantom hot spots are reduced by potentially illuminating less clutter. For this purpose the fixed meshgrid of 11m x 11m is replaced with a dynamic meshgrid of 5m x 5m around the rotation centre of the CoLORbot in every position under test. These sub-images are consecutively merged into the main image. For further analysis the already outlined track is split into clusters of 3 segments. The first cluster consists of the first 3 segments s1 - s3. The resulting images of both configurations are shown in Fig. 5.

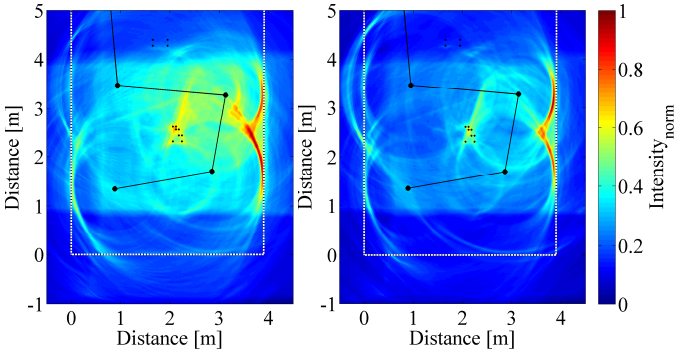

Figure 5. Clustered image of the segments s1-s3 with the omni-directional antennas in mono-static configuration (left) and bi-static configuration (right). Colorbar holds true for both images

The right image of Fig. 5 with bi-static configuration exhibits a higher level of signal to noise ratio and therewith a higher dynamic range. In both scenarios the right wall is highlighted more than the left wall, because the segment s2 is led in close distance. However, the object o1 to the left of the robot as well as the right wall exhibit quite similar round trip times (RTT). Due to the diverse configuration this ambiguity can be resolved in the bi-static configuration with less artefacts than in the mono-static configuration.

The next cluster consists of the segments s3 - s5 and is expressed in same manner in Fig. 6. Although the dynamic range is higher in the bi-static configuration a robust detection of the object o2 cannot be performed without a doubt in both cases. In the mono-static case the object is richly accompanied with clutter and in the bi-static case the object is shadowed with noise due to low dynamic range.

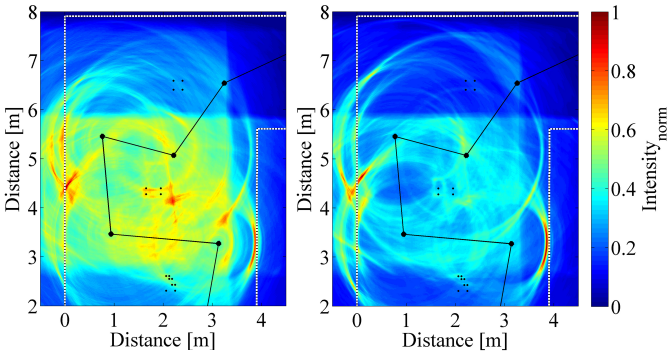

Figure 6. Clustered image of the segments s3-s5 with the omni-directional antennas in mono-static configuration (left) and bi-static configuration (right). Colorbar holds true for both images

In the third cluster which consists of the segments s5 -s7 the predominance of a bi-static configuration can clearly be seen. See Fig. 7 for the following discussion. Drastically reduced phantom hot spots and a higher dynamic range can be determined in the bi-static configuration. The object o3 can be extracted and a further track could be planned due to a interpretable image. In the mono-static case the object is massively shadowed with dense phantom hot spots.

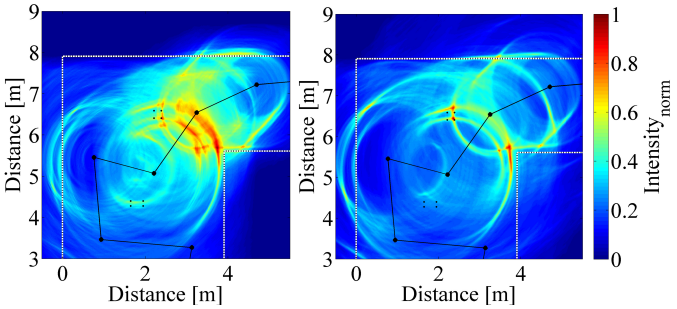

Figure 7. Clustered image of the segments s5-s7 with the omni-directional antennas in mono-static configuration (left) and bi-static configuration (right). Colorbar holds true for both images

The fourth cluster which consists of the segments s7 - s9 points out the distorting influence of an improper selection of the track. Results concerning this cluster are shown in Fig. 8. The track as well as the alignment of the antennas in bi-static configuration are the crucial key factor for a robust imaging. Finally, the synthetic aperture is generated by the motion. A non-diverse track generates a linear aperture. It is well-known that linear apertures are incapable to distinguish between half planes connected by this array in the middle. The phantom hot spot just occurs mirrored on the other side of the track.

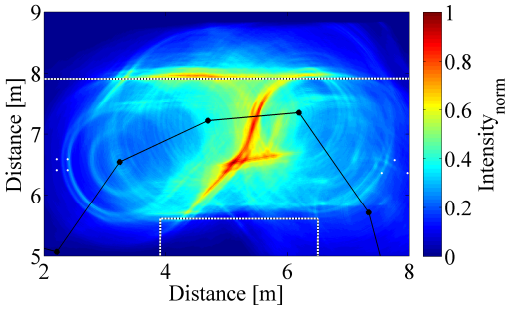

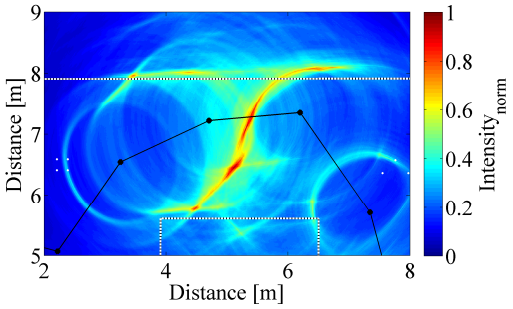

Figure 8. Clustered image of the segments s7-s9 with the omni-directional antennas in mono-static configuration (top) and bi-static configuration (bottom).

In both cases it can be seen that at the start of segment s6 the upper wall is imaged properly but simultaneously its phantom is mirrored on the other site of the track. Actually this type of artefact would also occur in the first cluster if there would be only the segment s2. However, the phantom hot spots in that case are resolved by the segments s1 and s3.

In the last cluster which consists of the segments s9 - s11 the same ambiguity cannot be resolved which results in distorting artefacts. The resulting image of this cluster can be seen in Fig. 9 for both configurations.

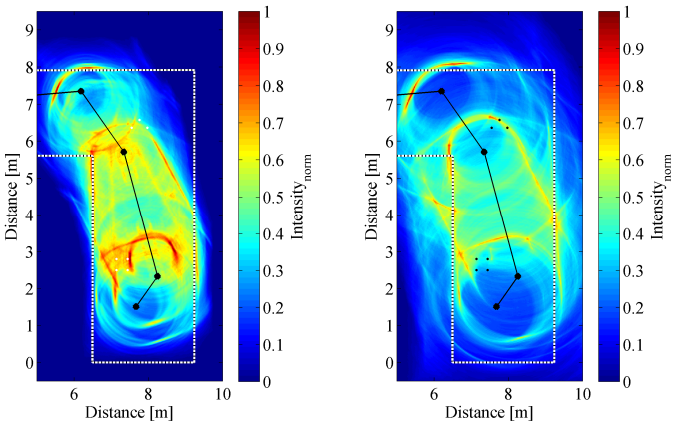

Figure 9. Clustered image of the segments s9-s11 with the omni-directional antennas in mono-static configuration (left) and bi-static configuration (right).

In both cases the left wall can be extracted but at the same time its phantom occurs symmetrically on the other side of the track. The object o5 can be recognised in the mono-static configuration more explicitly. This is because the antenna array is always orthogonal to the track and static. In this case one antenna shadows the reflection in bi-static configuration when it occurs from lateral direction (the radiating source lies in a straight line with both antennas).

d) Cross-Correlation Back Projection

As previously mentioned the cross-correlation back projection promises for robust suppression of artefacts subject to a proper local position of the reference node. To analyse its performance this modified KM algorithm was evaluated within the investigations. To arrange realistic circumstances an additional reference node was not implemented but rather measurement points of neighbouring segments were used. Concretely, the cross-correlation back projection algorithm was carried out for each segment with 2 reference nodes, i.e. the measurement performed in the middle position of the previous and subsequent segment. The reference nodes for the fifth segment s5 was the measurement in the middle of s4 and s6 and so on. Only s1 and s11 just had one reference node, i.e. from s2 and s10, respectively. Fig. 10 to Fig. 14 show the results of the cross-correlation back projection applied onto the bi-static configuration. On the left side previously shown images with classical KM and on the right side the cross-correlation back projection is shown.

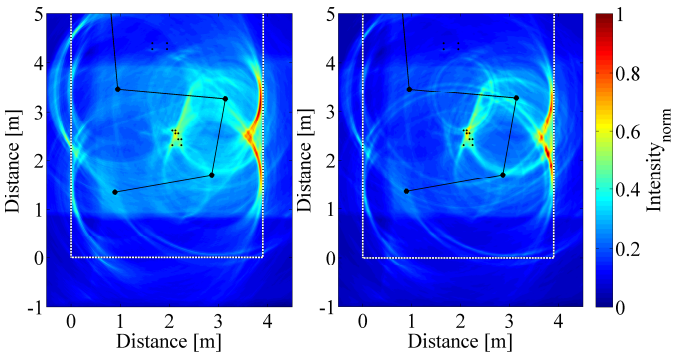

Figure 10. Clustered image of the segments s1-s3 with the bi-static configuration. With classical KM (left) and cross-correlation back projection (right). Colorbar holds true for both images

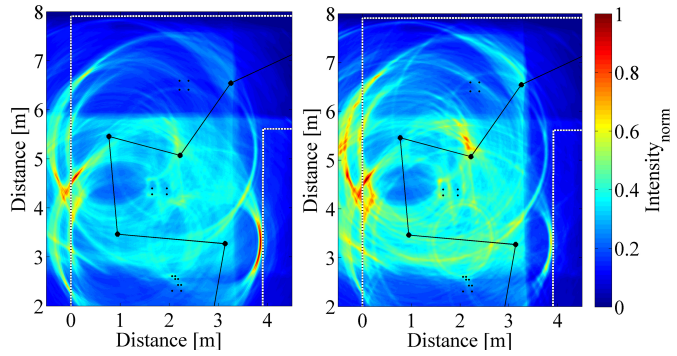

Figure 11. Clustered image of the segments s3-s5 with the bi-static configuration. With classical KM (left) and cross-correlation back projection (right). Colorbar holds true for both images

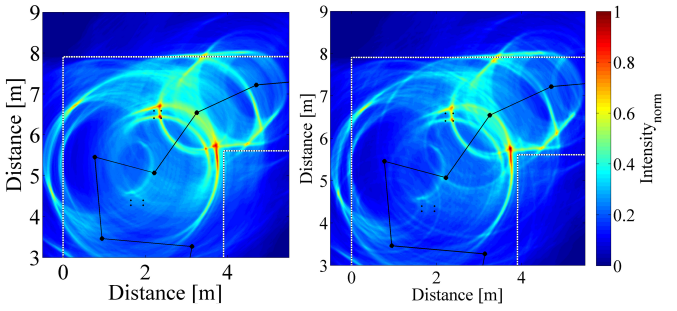

Figure 12. Clustered image of the segments s5-s7 with the bi-static configuration. With classical KM (left) and cross-correlation back projection (right). Colorbar holds true for both images

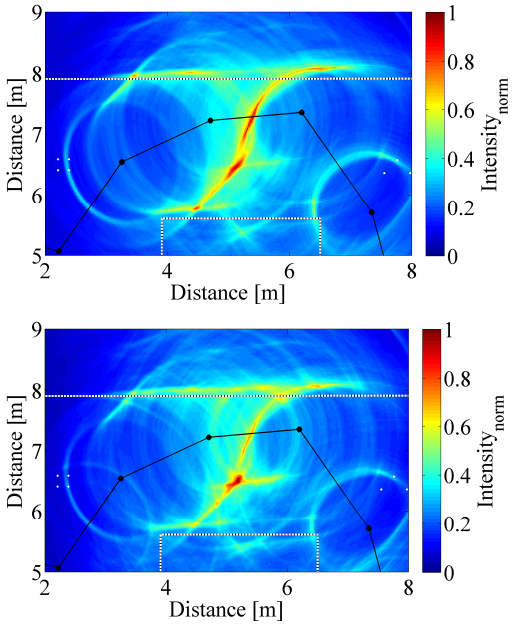

Figure 13. Clustered image of the segments s7-s9 with the bi-static configuration. With classical KM (left) and cross-correlation back projection (right).

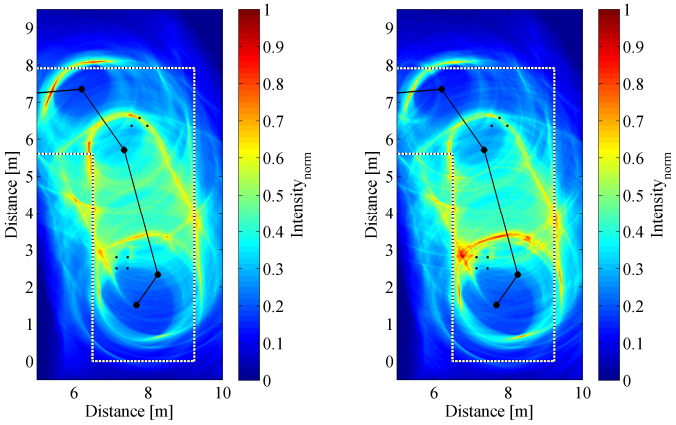

Figure 14. Clustered image of the segments s9-s11 with the bi-static configuration. With classical KM (left) and cross-correlation back projection (right).

In some cases the cross-correlation back projection can enhance the dynamic range effectively, e.g. in cluster 1 (Fig. 10) or cluster 3 (Fig. 12). In cluster 4 (Fig. 13) even phantom hot spots are suppressed. Whereas in cluster 2 (Fig. 11) and cluster 5 (Fig. 14) an enhancement of the image cannot be seen. However, it seems that the influence of the proper position of the reference node is of essential importance. Probably, static nodes with a priory known positions or an additional assisting robot with a sophisticated algorithm to estimate good positions will increase the potentials of cross-correlation back projection.

B. Performance Analysis of the Directive Antennas

Directive antennas have several advantages compared with omni-directional antennas. The previously mentioned Teflon embedded two tapered slot line Vivaldi antennas have a high gain of up to 15dBi throughout the whole bandwidth. This leads to higher signal to noise ratios and potentially higher dynamic range. Hence, imaging in case of a long distance of about several meters is quite feasible without a restriction to the adjacent area. With the 25° wide beam potentially less clutter is hit. A common parameter for the evaluation of antenna characteristics in time domain is derived from the antenna's transient response which is the peak value of the antenna impulse response. In the main beam the peak value of the directive antennas is by far higher than the peak value of the omni-directional antennas. A second time domain parameter is the so-called full width at half maximum (FWHM), which describes the broadening of the transmitted pulse due to the dispersion of the antenna. This value is also more advantageous at the directive antennas used here providing them a smoother shaper and less pulse duration. Oscillations in the antenna impulse response are quantified by the ringing duration parameter which is by far smaller at the directive antennas.

However, the main advantage of the directive antenna is also the reason for its disadvantage, i.e. the sharp 3 dB beam width of 25°. In many cases an immense effort for antenna alignment and regulating motions to properly gather spatially distributed energy in form of electromagnetic waves is needed. For a panorama view the antenna configuration needs to be rotated up to ten times resulting in ten measurements while this is performed with omni-directional antennas with just one measurement without the need of any motion. In worst case, the directive antennas will not recognize a nearby wall when they are improper aligned because the angle of reflection does not equal the angle of incidence with respect to the normal of the wall.

The directive antenna are throughout the investigation used in bi-static configuration positioned on the array with a distance of 0.15m to the rotation centre of the array, resulting in 0.3m distance to each other. At the beginning as well as at the end of each segment the robot stops and the array performs a full rotation while gradually makes measurements with the directive antenna arrangement. A dynamic meshgrid of 6m x 6m was used around each rotation centre. These 12 sub-images were merged together for the final image of the whole scenario. In Fig. 15 the result for classical KM is shown. Compared with the bi-static image of the omni-directional antennas (Fig. 4) the noise floor is extremely low resulting in very high signal to noise ratios. Actually, no artefacts or phantom hot spots can be seen. However, due to non-chaotic track and restricted number of measurement points (totally 12) some features can hardly be extracted, e.g. object o2, o4 and the walls to the left and right of segment s10. However, this is to some extent quite plausible and is not a criterion for error-proneness.

The signal to noise ratio could even be more enhanced by applying cross-correlation back projection but also on the expense of weak features which degrade more. For this purpose the previous and subsequent measurement points served as reference nodes. At the start and end the number of reference nodes was 1 (either the previous or the subsequent one). The cross-correlation back projection image is shown in Fig. 16.

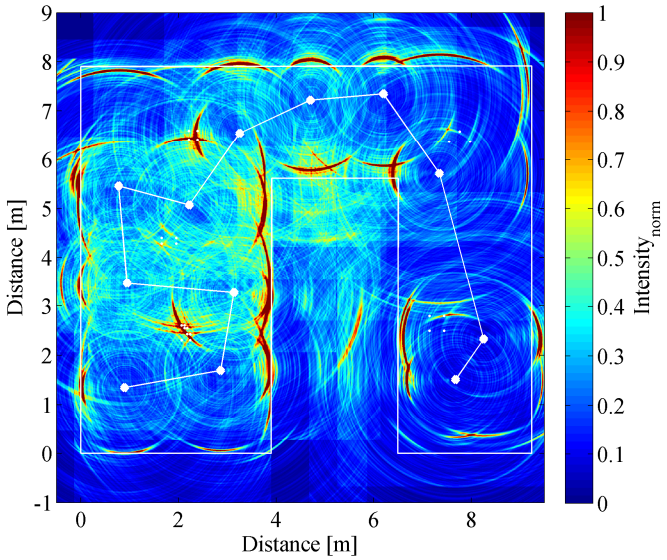

Figure 15. Full image with the directive antennas in bi-static configuration obtained with classical KM.

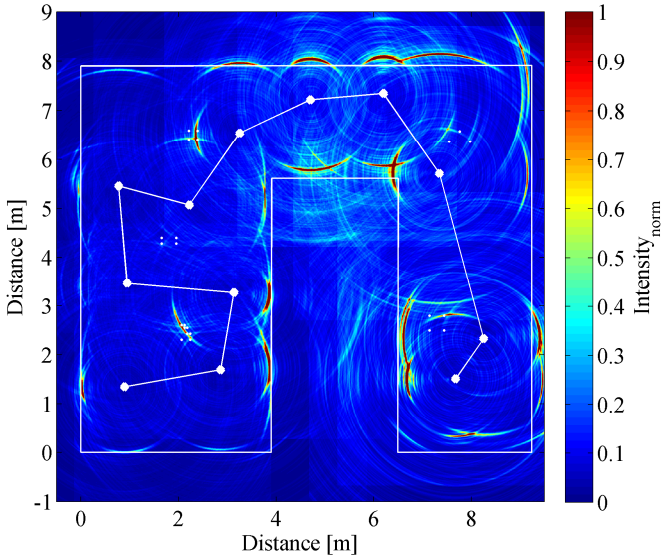

Figure 16. Full image with the directive antennas in bi-static configuration obtained with cross-correlation back projection

V. CONCLUSION

Environmental imaging by means of UWB technology performed by an autonomous security robot in an unknown indoor scenario is a resolvable challenge. Measurement results demonstrate the extraction of features like the structure of the room or solitary objects in sufficient quality for positioning purposes. The performance of omni-directional and directive antennas were analysed and compared to each other. Additionally, the cross-correlation back projection was analysed in comparison to classical KM. It is a more convenient strategy to use omni-directional antennas in a bi-static configuration. The naturally lower signal to noise and signal to clutter ratios (due to lower antenna gain) can be improved by using sharp beam directive antennas.

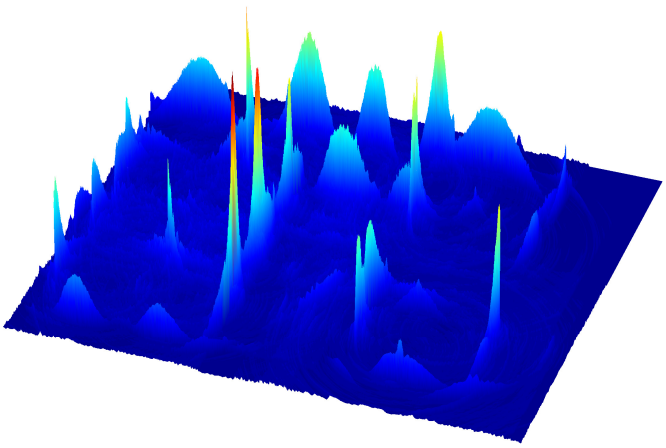

Figure 17. 3D altitude profile with the directive antennas in bi-static configuration obtained with cross-correlation back projection

However, this goes to the expense of restricted viewing angles. The cross-correlation back projection extremely depends on proper local selection of reference nodes. This decreases the practicability in real emergency scenarios. Most promising is the operation of a switched antenna array which consecutively combines both antenna types. A crucial factor is the robot track which should be a as chaotic as possible to generate a quite non-linear synthetic aperture. Future research can focus on the over-all improvement - e.g. improved imaging algorithms, reduction of data load and enhanced real-time capability, robust through-wall implementations etc.

ACKNOWLEDGMENT

The authors thank the Deutsche Forschungsgemeinschaft (DFG) for the support of the work as part of the “Cooperative Localisation and Object Recognition in Autonomous UWB Sensor Networks” (CoLOR) project within the UKoLoS priority program.

REFERENCES

[1] R. Salman, I. Willms. "3D UWB radar super-resolution imaging for complex objects with discontinous wavefronts." *IEEE International Conference on Ultra-Wideband (ICUWB),* Bologna, Italy, Sept. 2011.

[2] R. Zetik, H. Yan, E. Malz, S. Jovanoska, G. Shen, R.S. Thomä, R. Salman, T. Schultze, R. Tobera, I. Willms, L. Reichardt, M. Janson, T. Zwick, W.Wiesbeck, T. Deißler, J. Thielecke. "*Cooperative Localization and Object Recognition*" in UKoLoS Ultra-Wideband Radio Technologies for Communications, Localization and Sensor Applications. R.S. Thomä, R. Knöchel, J. Sachs, I. Willms, T. Zwick (Eds.). InTech Academic Publisher, ISBN: 978-953-307-740-6. in preparation.

[3] G. Shen, R. Zetik, Y. Honghui, O. Hirsch, R. Thomä. "Time of arrival estimation for range-based localization in UWB sensor networks." *IEEE International Conference on Ultra-Wideband (ICUWB),* 20-23 Sept. 2010

[4] J. Sachs, R. Herrmann, M. Kmec, M. Helbig, K. Schilling, “Recent Advances and Applications of M-Sequence based Ultra-Wideband Sensors,” ICUWB 2007 Singapore, September 24-26, 2007.

[5] R. Zetik, R.; J. Sachs, R. Thomä. "Modified cross-correlation back projection for UWB imaging: numerical examples." *IEEE International Conference on Ultra-Wideband (ICUWB),* 5-8 Sept. 2005.